Peer-reviewed version available at *Polymers* **2019**, *11*, 2045; doi:10.3390/polym11122045

Article

Revealing the influence of the degumming process in the properties of silk fibroin nanoparticles.

Guzmán Carissimi[1§], A. Abel Lozano-Pérez[2§], Mercedes G. Montalbán[3], Salvador D. Aznar-Cervantes[2], José Luis Cenis[2] and Gloria Víllora[1*].

[1] Department of Chemical Engineering, Faculty of Chemistry, University of Murcia (UMU), Campus de Espinardo (Murcia), 30100, Spain;
[2] Department of Biotechnology, Instituto Murciano de Investigación y Desarrollo Agrario y Alimentario (IMIDA). La Alberca (Murcia), 30150, Spain.
[3] Department of Chemical Engineering, University of Alicante, Apartado 99, 03080, Alicante, Spain.
§ Authors contributed equally.
* Correspondence: gvillora@um.es; (G.V.)

Abstract: In recent years, numerous research studies have shown the excellent characteristics of silk fibroin nanoparticles as a vehicle for drugs delivery and it is foreseeable that their production could reach industrial scale in the coming years. For this reason, it is essential to know all the parameters that affect the formation of nanoparticles in order to standardize the process. Several studies have stated that the process used for sericin removal (degumming) from silk cocoons has a strong impact in the silk fibroin integrity and their mechanical properties after processing it into biomaterials. In this work, silk cocoons were degummed following four standard methods: autoclaving, short alkaline (Na_2CO_3) boiling, long alkaline (Na_2CO_3) boiling and ultrasounds. The resultant silk fibroin fibers were dissolved in the ionic liquid 1-ethyl-3-methylimidazolium acetate and used for nanoparticle synthesis by rapid desolvation in polar organic solvents. The relative efficiencies of the degumming processes and the integrity of the resulting fibroin fibers obtained were analyzed by weight loss, optical microscopy, thermogravimetric analysis, infrared spectroscopy and SDS-PAGE. Particle sizes and morphology were analyzed by Dynamic Light Scattering and Field Emission Scanning Electronic Microscopy. The results showed that the different treatments had a remarkable impact on the integrity of the silk fibroin chains, as confirmed by gel electrophoresis which can be correlated with particle mean size and size distribution changes. The study confirm that all the parameters of the process must be controlled in order to reach an optimum reproducibility of the nanoparticle production.

Keywords: Silk Fibroin Nanoparticles, Cocoon Degumming, *Bombyx mori*, Ionic Liquids Ultrasound, Autoclave.

1. Introduction

For most medical applications of silk biomaterials, silk fibroin (SF) must be efficiently purified from silk cocoons (SC) by removing the silk sericin (SS) by means of an ancient process known as degumming, and this key step is commonly recognized as one of the most important procedures in the production of silk-based materials[1]. This purified SF can be dissolved in highly concentrated saline solutions such as LiBr 9.3 M [2] or Ajisawa's reagent ($CaCl_2$/EtOH/H_2O, 1:2:8 in molar ratio) [3], the most commonly used, but also in some ionic liquids, such as 1-butyl-3-methylimidazolium

chloride [4] or 1-ethyl-3-methylimidazolium acetate ([emim+][AcO-]) [5], which are recognized as efficient alternatives due to their interesting properties as green solvents [6–8]. Ionic liquids, with a halogen or a small carboxylate anion, are capable of breaking the network of intra- and intermolecular hydrogen bonds and thus dispersing the peptide chains of the SF[9]. The conventional dissolution of SF in highly concentrated salts is a time-consuming multistep process that involves dialysis against distilled water for several days in order to remove the salts and obtain an aqueous solution of SF[10] prior to their regeneration in solid state in the form of SF nanoparticles (SFN) [3]. Furthermore, the aqueous SF solution obtained after dialysis is relatively unstable at 4 °C, evolving to a hydrogel due to changes in the pH of the solution or a change in pressure or shaking [11,12]. Alternatively, the ionic liquid-SF solutions can be precipitated directly into nanoparticles [5,13] avoiding the dialysis step and giving more stable SF solutions.

Silk sericin comprises a water-soluble globular protein family that are soluble in hot or boiling water due to their amino acidic composition, with an abundance of mostly polar amino acids such as serine or aspartic acid [14]. The degumming process can be performed using different methodologies that are based on the differences in solubility between both SS and SF. In general, a hot aqueous medium is used as extracting medium, preferably alkaline, in which SS is soluble and thus is separated from SF fibers, which remain essentially insoluble under these conditions. Several degumming methods have been reviewed recently showing the effect of this critical processing step on the structure and properties of SF for multiple applications [15–24]. Among the different methods, the use of an autoclave in different configurations is frequently mentioned: in an aqueous solution subjected to 121 °C for 20 minutes [15] or using water vapor generated in the autoclave [17]. Although this method presents a lower yield than the protocols that use alkaline boiling, it has the advantage of lower production costs while maintaining acceptable the mechanical characteristics of SF fibers and is very useful when trying to recover salt-free SS by spray-drying [25,26]. Probably, the most used degumming method for biomedical applications of silk fibroin is that involving boiling the cocoons in alkaline solution (Na_2CO_3 0.02N) for 30 minutes [27]. This method extracts SS very well and involves low SF degradation, which makes it useful for applications where high purity and strong integrity of SF is needed. Other methods have also been described in which boiling is used for longer times, e.g., 120 minutes [28], or by extraction in hot water assisted by ultrasound [23] or using a solution of 8M urea at 80 °C for 120 minutes [15]. Also, experimental works on the removal of SS by different proteases enzymes [21][29] or organic acids, such as tartaric acid, have also been seen to perform efficiently [30][31].

Previous studies have found that different degumming processes affect SF yarns properties [15,23,24,32,33] and also concern the production of SF-based engineered materials like films [34–36], 3D scaffolds[28] or electro-spun mats[27,37]. However, to the best of our knowledge, no study on how the degumming process affects SFN formation, their structural characteristics and the changes in their size, Z-potential and surface charge density have been carried out. All these characteristics would affect the efficiency of SFN as drug delivery systems.

Several research studies have shown the excellent characteristics of SFNs as a vehicle for drugs and biomolecules[38–41], so their production will presumably reach industrial scale in coming years. For this reason, it is of great interest to know all the parameters that affect the formation of nanoparticles to standardize the process and control their features.

Following a priority research line of our lab that attempts to delve into the effects of all the stages of silk processing in the properties of the biomaterials, specifically focused on the reproducibility of the processes,[13,42–44], the present study focuses on how the degumming process affects SFNs structural features (morphology, size distribution, Z-potential and surface charge density). In order to assess the different silk degumming processes and their possible effect on SFNs, silk was degummed by means of four different methods, namely autoclaving (D1), alkaline treatment with Na_2CO_3 for 30 minutes (D2) or 120 minutes (D3) and a high-power ultrasound treatment (D4). Each SF obtained by the mentioned degumming methods was used to prepare SFN. The effectiveness of the degumming process was assessed by the weight loss. Protein integrity after the different degumming processes and dissolution in ionic liquid was studied by Sodium Dodecylsulfate-Polyacrylamide Gel Electrophoresis (SDS-PAGE). A morphological observation of SF fibers after the degumming processes was made by Optical Microscopy and Scanning Electron Microscopy (SEM). The thermal stability of the SF fibers was measured by Thermogravimetric Analysis (TGA). The changes in the secondary structure of the protein were monitored by the crystallinity index (CI%) of the sample obtained from Fourier transformed infrared spectroscopy (FTIR) analysis. Finally, the morphology, size distribution, Z-potential and surface charge density of the obtained nanoparticles were analyzed by Field Emission Scanning Electron Microscopy (FE-SEM) and Dynamic Light Scattering (DLS), respectively.

2. Materials and Methods

2.1. Materials

Silk cocoons (SC) were obtained from silkworms *Bombyx mori* reared in the sericulture facilities of IMIDA (Murcia, Spain) and raised on a diet of fresh natural *Morus alba L.* leaves. Cocoons were then stifled to kill the pupae by means of dry heat (85 °C) [45]. The intact chrysalides were extracted manually from the cocoons prior to silk processing. All reagents and solvents were purchased from Sigma-Aldrich (Madrid, Spain) with the exception of methanol (Honeywell, Germany) and 1-ethyl-3-methylimidazolium acetate ([emim$^+$][AcO$^-$]) 95% (Iolitec, Germany).

2.2. Degumming methods

In this work, four degumming methods were chosen among the most representative of the commonly used in literature and were named as: D1) Degumming by autoclave [15]; D2) Degumming by short alkaline boiling (30 min) [27]; D3) Degumming by long alkaline boiling (120 min) [28]; D4) Ultrasonication with probe in water [23]. A brief overview of the four methods with the most representative features can be found in Table 1. For comparative purpose, the liquor ratio of SF in each solvent was kept at 1:200 (w/v) for all methods.

Table 1. Overview of the used degumming methods.

Reference	Process	Solvent	T (°C)	Time (minutes)
D1	Autoclave	MilliQ water	121	30
D2	Short Alkaline Boiling	Na_2CO_3 0.02N	100	30
D3	Intensive Alkaline Boiling	Na_2CO_3 0.02N	100	120
D4	Ultrasonication with probe*	MilliQ water	60	60

*Branson Sonifier SFX-550 equipped with a disruptor horn and a 1/8″ diameter tapered microtip. Sonication was set for 30 minutes with 50 % amplitude and the maximum temperature was set at 60 °C.

After each degumming process, the remaining SF of each batch was washed twice with 1.5 L of distilled water at 60 °C for 5 min to remove any unbound SS. The obtained SF was dried for 24 h in a fume hood until constant weight. The weight loss after the different degumming methods was calculated as:

$$Weight\ loss\ (\%) = \left[1 - \left(\frac{dry\ mass\ of\ SF}{dry\ mass\ of\ native\ cocoons}\right)\right] * 100, \quad (1)$$

2.3. Preparation of Silk Fibroin Nanoparticles

The preparation of SFNs was based on the method described by Montalbán *et al*. [5]. In brief, silk fibroin fibers obtained from the different degumming methods were dissolved in [emim$^+$][AcO$^-$] (10 wt. %) by using high-power ultrasounds. To reduce the viscosity of the mixtures, 3 mL of MilliQ water (18 mΩ/cm) were added to 5 g of the SF-[emim$^+$][AcO$^-$] solution and then heated to 60 °C. Subsequently, the mixture was sprayed as an aerosol by a thermostatically controlled 0.7 mm two-fluid nozzle (from a Mini Spray Dryer B-290, BÜCHI Labortechnik, Flawil, Switzerland, Part No. 044698) with compressed N_2 (1 bar) onto 100 mL of cold methanol (-20 °C) gently stirred. The resultant suspension was stirred for 2 hours and the nanoparticles were separated by centrifugation and subsequent washing steps with methanol (1x) and water (3x) and freeze dried by using an Edwards Modulyo 4K Freeze Dryer at -55 °C and 0.5 mbar for 72 hours. Methanol and [emim$^+$][AcO$^-$] were recovered and purified from the supernatant by simple distillation.

2.4. Sodium dodecylsulfate-polyacrylamide gel electrophoresis (SDS-PAGE)

Electrophoresis was performed on the obtained SF solutions in [emim$^+$][AcO$^-$] according to the Laemmli protocol [46] in order to compare the protein integrity after the different degumming processes. The different samples of SF dissolved in the ionic liquid, as described above, were diluted (1%) with MilliQ water and mixed with loading buffer (1:1) containing β-mercaptoethanol (10% v/v) and heating the mixture at 95 °C for 5 min for protein denaturation. Next, protein concentrations were unified at 50 μg per lane of sample. The electrophoresis was performed following the protocol described by the manufacturer on an Amersham ECL Gel horizontal electrophoresis system (Code No. 28-9906-08) connected to a BioRad Power supply (100 V), by using an acrylamide gel with a 4-20 wt.% gradient for better protein resolution (Amersham GE, Code No. 28-9901-59) and an Amersham ECL Gel Running buffer, 250 mL (Code No 28-9902-52). An aliquot of 5 μL of ColorBurst™

Peer-reviewed version available at Polymers 2019, 11, 2045; doi:10.3390/polym11122045

Electrophoresis Marker (Sigma-Aldrich, St. Louis, MO) was loaded as reference. After electrophoresis, the gels were stained with 0.25% Coomassie Brilliant Blue (Across Organics, Belgium), destained in ethanol/water mixture and photographed for analysis.

2.5. Morphological, physicochemical and structural characterization of SF fibers and SFNs

Optical microscopy images of the SF fibers obtained were taken with a Nikon Eclipse 50i fluorescence microscopy equipped with Plan Fluor objectives (5x and 100x), fluorescence filters for DAPI (UV-2E/C), FITC (B-2E/C) and TRITC (G-2E/C), and a 100 W mercury lamp as fluorescence light source. Images were captured by a Nikon DS-Fi1-U2 camera controlled by the NIS-Elements F software (Ver. 3.00, SP7, Build 547).

For the morphological characterization of the SF and the SFN, SEM and FESEM images were recorded by a JEOL JSM 6100 (Tokyo, Japan) and Thermo Scientific Apreo S (Brno, Czech Republic), respectively. For the SF samples, fibers were stuck on an aluminum stub with a thin self-adherent carbon film and later sputtered with gold. The SEM was operated at 20 KV. For SFNs, a diluted SFN dispersion was dropped on a mica disc (Ted Pella, inc. V1 highest grade) air dried and later sputtered with platinum for 5 minutes resulting in a 5.13 nm film thickness (Leica, EM ACE600, Leica Microsystems Inc, Concord, ON, Canada). Mica discs were pretreated by removing the upper layers with scotch tape three times before placing the sample.

The thermal properties of SF were measured by thermal gravimetric analyzer (TA instruments, SDT 2960 simultaneous DSC-TGA, Waters LLC, USA) in a temperature range of 25−800 °C with a heating rate of 10 °C /min under an inert nitrogen atmosphere in an open bin. Weight loss and heat flow were simultaneously recorded and plotted against temperature for Thermogravimetric Analysis (TGA) and Differential Scanning Calorimetry (DSC), respectively.

Infrared spectral data obtained by Attenuated Total Reflectance Fourier Transform Infrared Spectroscopy (ATR-FTIR) were collected in order to compare the effect of the different degumming processes in the secondary structure of the fibers. The calculation of the Crystallinity index (CI%) and the changes in the band fitting of the Amide I region, (1600−1700 cm^{-1}) of the spectra were chose as the most informative for this purpose [47,48]. ATR-FTIR spectra were recorded in a Nicolet iS5 spectrometer coupled to a diamond crystal iD7 ATR module (Thermo Fischer Scientific, USA). OMNIC Software V9.9.471 was used for controlling the equipment and the post processing of spectral data, including baseline and ATR corrections. Measurements were made with a resolution of 4 cm^{-1} in the spectral range of 4000-550 cm^{-1} by collecting 64 scans using N-B strong apodization and mertz phase correction. A background was collected before each spectrum measurement with the crystal window clean and uncovered. FTIR spectra were recorded in three different samples of the SF fibers to ensure reproducibility. All samples were vacuum dried prior to assessment to minimize the contribution of water to the spectra.

The CI% of the SF samples was calculated using the following equation:

$$Crystallinity\ Index\ (CI\%) = \frac{A_{1260}}{A_{1235}} \times 100, \quad (2)$$

Where A_{1260} and A_{1235} represent the measured absorbance at 1260 and 1235 cm^{-1} respectively, after performing a base line correction (See an example at Figure S1, from the electronic supplementary information).

Complementarily, the secondary structure of the SF samples was also assigned by band fitting of the Amide I region, (1600−1700 cm^{-1}) of the spectra by using OMNIC V9.9.471 software following the approach described by Hu *et al.*[49]. Firstly, a baseline and advanced ATR corrections for one bounce of the incident light at an angle of 45° and a refractive index of 1.60 for the sample were applied to the original spectrum. Then, Fourier Self-Deconvolution (FSD) was applied to the Amide I region as a band narrowing technique. The parameters for the FSD were chosen on the basis of the resolution of the overlapping spectral features. The minimum values of the second derivative of the spectrum obtained by the FSD were used to center the initial bands of Gaussian shapes. Then, the iterative fitting algorithm implemented in the software was used to minimize the residual value between the spectrum and the sum of the deconvoluted bands without baseline. Finally, the resulting Gaussian bands were area-normalized and the relative area of the individual bands was assigned to the secondary structure of the protein according to the position of the peak, as can be observed in Table S1 of the electronic supplementary information. The aforementioned calculation was made assuming that all the C=O stretching vibrations have the same excitation coefficient, which means that their areas are proportional to the fraction of each secondary structural component [50]. An example of the band assignation can be found in the Figure S2 of the electronic supplementary information.

The characterization of the nanoparticles regarding their size and surface characteristics were performed by dynamic light scattering by using a Malvern Zetasizer Nano ZSP (Malvern Intruments Ltd, UK), equipped with a laser of 4 mW power and 633 nm wavelength. Intensity weighted mean hydrodynamic diameter, expressed as Z-Average, and Z-potential were measured by DLS and phase analysis light scattering (PALS) techniques, respectively. Samples were seen not to absorb at 633 nm in measurement conditions. A 1 mg/mL SFNs suspension was prepared by ultrasonication for 1 min at 30 % amplitude with pulses of 15 s before loading into the disposable capillary cell for Z-potential (DTS1070, Malvern). The backscattered light was measured at 173° relative to the source after 120 seconds of equilibration time at 25°C. The integrated Malvern software calculates the Z-Average and size distribution from fitting the autocorrelation function by CUMULANT analysis and multiple exponential decays by non-negative least square (general purpose under Malvern software options), respectively. Size results shown are the average of 3 measurements, were each measurement consisted of 12 runs of 10 seconds with no delay between measurements. The Z-potential was calculated through Henry´s equation using electrophoretic mobility of SFNs. Smoluchoski approximation ($\kappa\alpha = 1.5$) was assumed. Z-potential results are the average of 6 measurements taken in a fully automated way by the software with a minimum of 12 runs.

The surface charge density (σ) of a spherical colloidal particle can be obtained following the method proposed by Makino, K., & Ohshima, H. (2010) on the basis of the Z-potential and the ionic strength of the medium [51]. For a nanoparticle with constant surface charge density, the surface charge density is a more characteristic quantity than the Z-potential, ψ_0, because for such particles the Z-potential is not a constant and depends on the electrolyte concentration. The method is based on the following equation:

$$\sigma = \frac{2\varepsilon_r \varepsilon_0 \kappa k T}{ze} \sinh\left(\frac{ze\psi_0}{2kT}\right)\left[1 + \frac{1}{\kappa a}\frac{1}{cosh^2(ze\psi_0/4kT)} + \frac{1}{(\kappa a)^2}\frac{8\ln\left[\cosh\left(\frac{ze\psi_0}{4kT}\right)\right)}{sinh^2(ze\psi_0/2kT)}\right]^{\frac{1}{2}} \quad (3)$$

where κ is the Debye-Hückel parameter defined by:

$$\kappa = \left[\frac{1000e^2 N_A(2I)}{\varepsilon kT}\right]^{1/2} \quad (4)$$

and k is the Boltzmann constant, T is the absolute temperature, $\mathcal{E}_r$ is relative permittivity of the solvent, $\mathcal{E}_0$ is the permittivity of the vacuum, $\mathcal{E}$ is the permittivity, N_A is the Avogadro's number, e is the elementary electric charge, I is the Ionic strength; a is the radius of the spherical nanoparticles, Ψ_0 is the Z-potential and z is the electrolyte valence.

All the parameter values used for the calculation of the surface density charge are shown in the Table S2 of the Supplementary Information.

2.6. Statistical analysis

Data were presented as mean ± SD (standard deviation), calculated from three independent samples per condition by using Graphpad Prism 8.0.1 software. As normality (Kolmogorov-Smirnov, $p > 0.05$) and homoscedasticity (Levene, $p > 0.05$) were met, the statistical significance was determined using the parametric tests of Tukey ($p < 0.05$) and ANOVA ($p < 0.05$) for the comparisons of two or more groups, respectively.

3. Results and Discussion

3.1. Degumming results

The raw SC and the SF obtained after the degumming process, were weighed and their mass differences are presented in Table S3 (supplementary information). From the results, the weight loss follows the series D4 < D1 < D2 < D3. The D1 and D2 methods achieved similar weight loss of 31.3 and 32.4%, respectively. The D3 method represents a remarkable increase in the severity of the treatment in terms of time with respect to D2 and the weight loss reached 44.4%, the highest of the different tested methods. D4 method yielded the minor loss of mass, with only 25.9%. Assuming that only 25-30% of the total weight in the cocoons corresponds to the SS fraction [14,52,53], we can infer that not only sericin but also fibroin have been lost in the D3 treatment, probably due to the degradation of the fibers with this severe processing conditions and fibroin fiber loss during the process.

3.2. SF Secondary Structure Analysis

CI(%) determination by ATR-FTIR spectroscopy is a useful tool for assessing the effect of the degumming process due the remarkable differences of the SS and SF secondary structures [54], which are translated to the different signals in the amide III band [55,56]. The CI values were expected to increase as SS is removed due to the fact that SF presents a more ordered structure than SS [57,58]. The CI% was calculated with the ratio of the absorption bands at 1260 cm^{-1} (Crystallinity, β-sheet) [59] and 1235 cm^{-1} (amorphous, random coil) [60] bands. Results for the CI% of the different samples

are shown in Table S2. As can be seen, the CI for the external and internal faces of the SC were 49.3 and 50.7 %, respectively. All SF samples showed an increase in CI with respect to the raw silk cocoon, as expected. Not surprisingly, SF-D1 and SF-D3 presented the highest CI, both 59 %, but, in our opinion, due to different factors. On the one hand, the alkaline carbonate treatment has the potential to partially degrade the SF fibers, especially those regions with lower crystallinity, resulting in an increase in the overall CI%, an effect previously reported in literature [45]. This result is in accordance with the highest mass loss among samples (44.4%) observed during the treatment. On the other hand, the autoclave process with high pressure and temperature would induce an increase in the overall β-sheet content through a process of internal rearrangement of the chains facilitated by water molecules also described by Xu *et al* [61]. The D2 method had a moderate increase in terms of CI (56%) compared to D1, with a similar mass loss. The ultrasound-degummed SF showed the lowest CI (52%), which correlates well with the fact that it is the sample with the lowest weight loss (25.9%) and probably SS are still adhered to the surface of the SF lowering the overall CI%.

In order to investigate the effect of the degumming process on SFN formation, the Amide I infrared absorption band was chosen as a marker of the secondary structure of SF, following the procedure described in Section 2.5. The secondary structure features of the degummed SF are summarized in Figure 1 and Table S3, along with a statistical comparison (two-way ANOVA), in the electronic supplementary material.

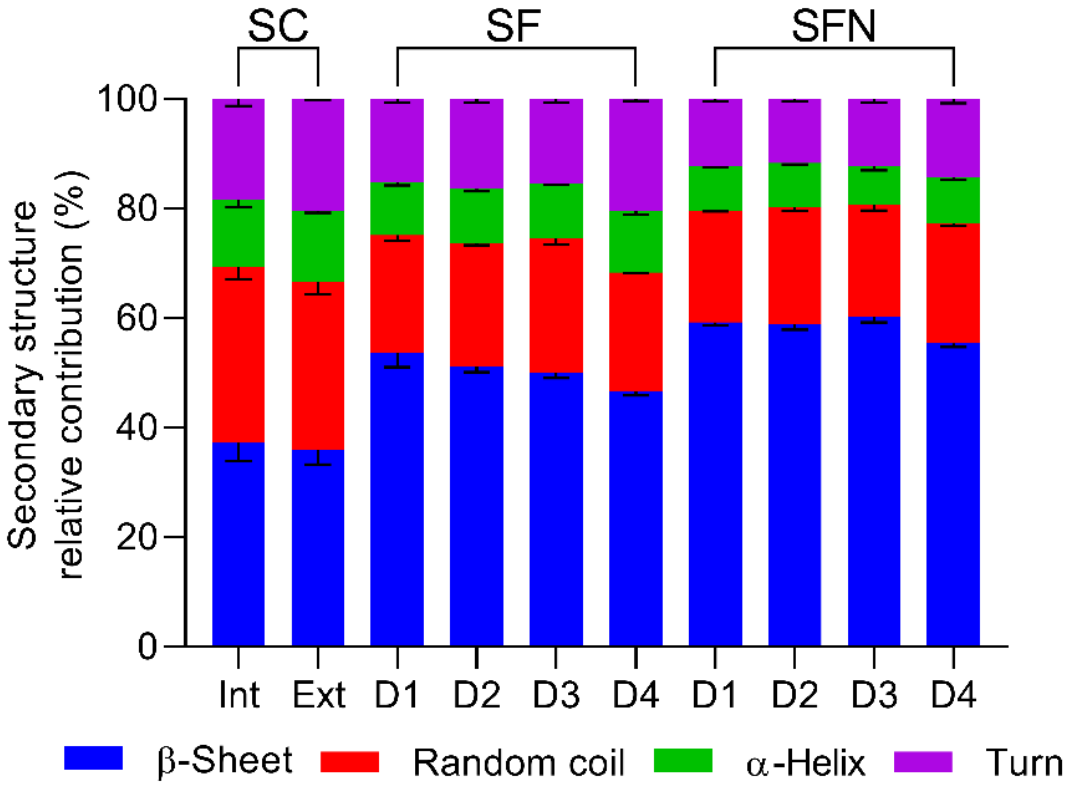

Figure 1. Secondary structure relative contribution of the silk cocoons and silk fibroins in the different stages of the process, obtained by FSD analysis of the Amide I infrared absorption band. SC) Silk Cocoons, internal or external faces, SF) Degummed silk fibroin and SFN) Silk fibroin nanoparticles prepared from SF degummed by: D1) Autoclave, D2) Na_2CO_3 30′, D3) Na_2CO_3 120′ and D4) Ultrasound. *(Please refer to the online version for the color representation of the figure.)*

After the degumming process of the SC, the random and α-helix structures were largely reduced while the β-sheet content (%) increased in all SF samples due to the removal of the SS. Resultant values agree with the previously proposed for SF [49,62,63]. SF-D1 showed the highest β-sheet

content. As was stated before, the severe conditions of pressure and temperature would induce certain internal rearrangement of the chains, promoted by water molecules, resulting in an increase of β-sheet [61]. No statistical differences could be seen in β-sheet content between SF-D2 and SF-D3 while SF-D4 presented the lowest amount of β-sheet. SF-D2 and SF-D3 samples presented the highest relative percentage of random coil structure with 22.4 and 24.5 %, respectively.

When processing the SF into SFN, the overall β-sheet structure increased while the rest of secondary structures were reduced for all samples, in agreement with similar works [45]. It could be hypothesized that the relative increase in the β-sheet content may be caused by degradation of the amorphous regions in peptides of low molecular weight. Therefore, the small peptides of the protein could be lost during the SF coagulation and subsequent washing steps.

Interestingly, the β-turn structures, which are short hydrophilic chains that connect the β-sheet strands, showed the highest reduction among all secondary structures. This finding suggests that during the dissolution of the SF in ionic liquid and later nanoprecipitation in methanol, these β-turns peptides were partially lost.

SFN-D1, -D2 and -D3 showed similar relative amounts of secondary structure. However, SFN-D4 showed a higher content of β-turn and random coil, which might be due to two different reasons. On the one hand, it could be due to the presence of SS in the SFN coming from the remaining SS in the SF-D4 fibers. On the other hand, if almost all the SS had been removed during the overall process and washing steps, the SS present in the ionic liquid solution might have interfered in the molecular arrangement during SF recrystallization in the nanoparticles , leading to a decrease in the total β-sheet content as previously described by Lee *et al*. [36].

3.3. Optical and electronic microscopy

The differences in the integrity of the SF fibers after the different degumming treatments were studied by optical microscopy and SEM images. As can be seen in Figure 2, there are notable differences in the surface of the SF fiber, due to the relative damage suffered during each treatment.

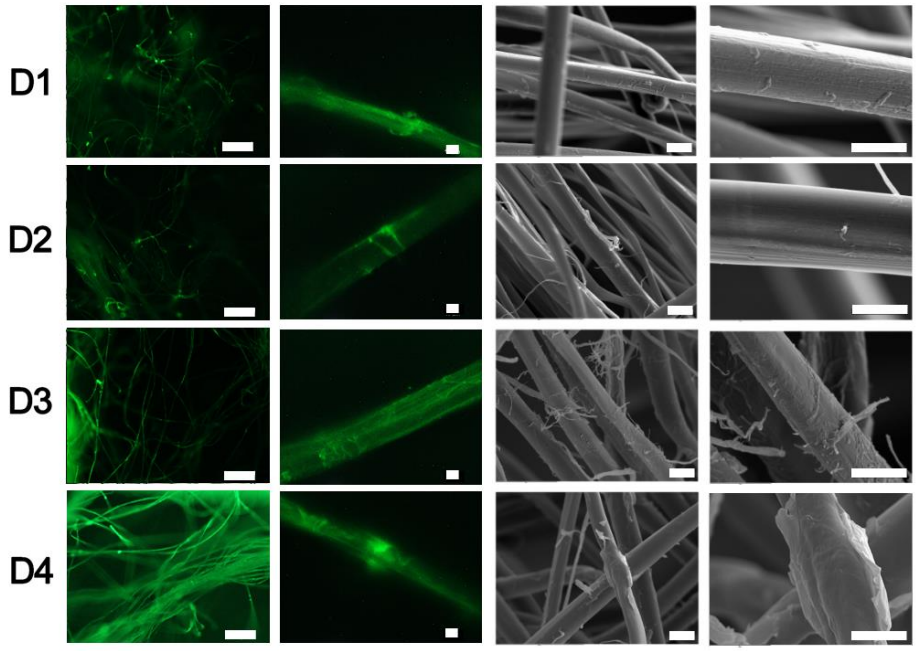

Figure 2. Comparative images obtained with the optical fluorescence microscope with fluorescein isothiocyanate (FITC) filter at different magnifications (scale bar: 500 μm for the first column and 10 μm for the second column) and scanning electron microscope of the degummed SF from the following degumming process at different magnifications (scale bar: 50 μm for the third and fourth column). D1) Autoclave, D2) Na_2CO_3 30′, D3) Na_2CO_3 120′ and D4) Ultrasound. *(Please refer to the online version for the color representation of the figure.)*

The images of the SF samples at different magnifications under ultraviolet light using a FITC filter presented visible differences in the brightness of the fibers. As SS has a higher fluorescence than SF [64], the bright green spots on the surface of the fibers could be remaining SS.

In the SEM images it can be observed that degummed SF-D1 sample showed a loss of fibers with a mostly smooth surface but small remains of SS are still attached to the SF fibers. The SF-D2 sample presented a moderate number of unraveled microfibers while presenting the smoothest surface, almost completely free of SS. The degummed SF-D3 sample revealed a highly damaged structure, with no clear signs of SS but fully coated with detached microfibers. These irregularities on the surface of the fibers scatter the light in the microscopy images and reflect the intense degradation produced by this degumming method. The SF-D4 sample presented neither unraveled microfibers nor a smooth surface, which would be due to the presence of SS, as reported previously [65][66].

3.4. Sodium dodecylsulfate-polyacrylamide gel electrophoresis (SDS-PAGE)

The molecular weight (M_w) of the SF chains in the degummed samples has been studied by gel electrophoresis and correlated with the integrity of the SF chain after the different degumming methods. Each degummed SF was dissolved in [emim$^+$][AcO$^-$] with the aid of high-power ultrasounds [13], samples were loaded and run in an SDS-PAGE electrophoresis gel, and the result is shown in Figure 3. Native SF consists of a heavy chain (H), a light chain (L) and a glycoprotein (P25) and their respective molecular weights are 391, 26 and 24 kDa (30 kDa including the *N*-linked oligosaccharides). The H and L-chains are bonded together by a disulfide bridge [67] and complexed with P25 in a 6:6:1 molar ratio [68]. This protein, P25, was only slightly visible in the electrophoresis gel (Figure 3) in the lane of SF-D4.

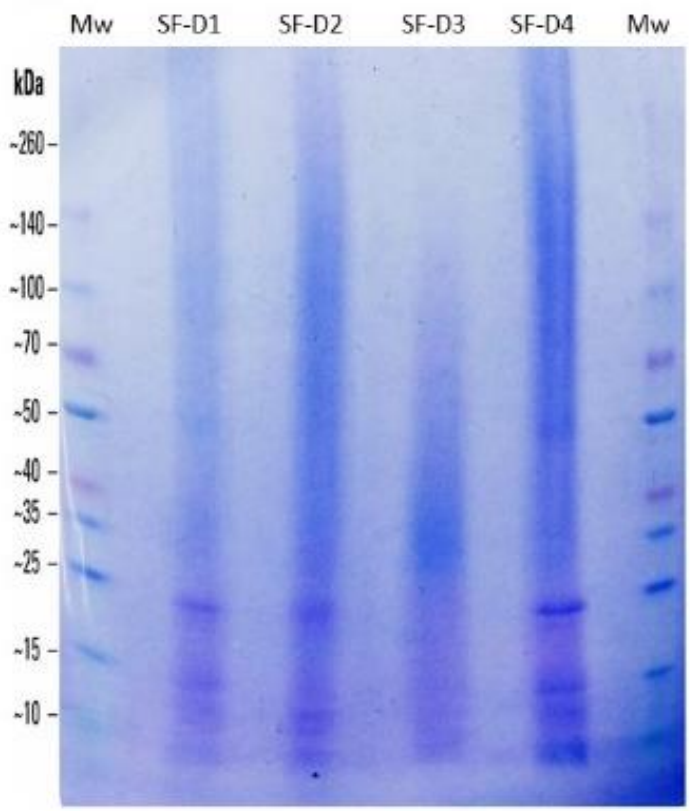

Figure 3. SDS-PAGE analysis of the protein components of SF after the different degumming process, namely: D1) Autoclave; D2) Short alkaline boiling; D3) Intensive alkaline boiling and D4) Ultrasonication probe. Lane *Mw*: Spectra Multicolor Protein Ladder 10–260 kDa (Thermo), (4–20% gradient Gel Amersham GE-HC). *(Please refer to the online version for the color representation of the figure.)*

The studied SF samples presented large differences between them, as seen by electrophoresis. SF-D1 showed a light smear along the whole lane and clear bands at 26 and 15 kDa can be observed. SF-D2 appeared as a smear of peptide sizes from 140 kDa downwards; the L-chain of fibroin is clearly visible at 26 kDa. SF-D3 presented a size distribution as a smear between 100 and 10 kDa with a darker zone in the 30-40 kDa and no bands were detected at 26 or 24 kDa. SF-D4 showed a heterogeneous smear along the whole line with darker zones at 140, 100 and 50 kDa and clear bands at 26 and 15 kDa.

The smears in the upper-middle molecular weight distribution can be interpreted as fragments of the H-chain as a result of the degradation from the degumming process [25]. The SF-D1 was seen to be the least aggressive treatment for SF, which is denoted by the light smear with only a small fraction of H-chain degraded, while the major fraction of the protein could not enter the gel due the size of the chains. On the other hand, the L-chain of 26 kDa is clearly evident, which accentuates the hypothesis of the SF-D1 treatment producing lower SF degradation. Similar results for autoclave degumming have been published [15]. SF-D2 and SF-D4 presented a moderately dark smear in the top portion of the gel (ca. 260-50 kDa) similar to that previously described [13], with bands at 120 kDa (SS) [69], 50 kDa (H-chain of SF), 35 kDa (H-chain of SF), 26 kDa (L-chain of SF) and 15 kDa (SS) [14]. The collections of bands and the smear at the top portion of the gel confirmed the SF H-chain degradation and remaining SS, as seen in the optical and electronic microscope images. This was especially evident for SF-D4, reflecting the SEM images (Figure 2) and the low CI%. SS comprises a big family of proteins and they can be classified into three groups according to their position in the fiber,-the outer, the middle and the inner layers. The inner layers contain the smallest and the least water-soluble proteins. Theses inner layers of SS have a molecular weight of 14.4 kDa[14]. The bands at 15 kDa seen in SF-D1, SF-D2 and SF-D4 could correspond to these inner SS proteins. This fact correlates with the optical microscopy images, where SF-D1 and SF-D2 showed the remains of small still attached SS and SF-D4 presented bands of SS with heavier molecular weights. Among the treatments studied, alkaline boiling for 120 minutes produced the largest degradation of the H and L-chains, as no signs of high molecular weight fragments (> 100 kDa) or light chain band at 26 kDa could be identified. This treatment clearly narrows the distribution of molecular weight sand concentrate them in the bottom portion of the distribution range.

Through an analysis of the gel, we conclude that the different degumming treatments produced different degrees of degradation of the SF chains: D1< D4 < D2 < D3. Thus, the alkaline boiling for 120 minutes appeared to be the most aggressive process for t SF degumming, which agrees with other authors [17], [32].

3.5. Thermal properties

The obtained results for TGA of the SC and the SF fibers after the four different degumming process are depicted in Figure 4, along with thermal the decomposition rate temperature (T_{dm}) denoted by the peak of the first derivate. T_{dm} corresponds to an endothermic transition (negative peak of DSC curve). The mass loss in the first transition at T < 100 °C, were due the evaporation of water content. As can be seen, in all cases the weight residue percentage is reduced sharply after 315-319 °C due to the degradation of SF, which is attributed to thermal degradation of β-sheet ordered structures [70]. Both mild degumming methods for SF (D1 and D2) showed equal T_{dm} of 319 °C. Fibers degummed by the more aggressive treatments, D3 and D4 processes, showed the lowest T_{dm} at 316 °C and 315 °C respectively. Interestingly, the cocoon sample showed a significantly higher T_{dm} reaching 330 °C (Figure 4a). This higher thermal stability of the cocoon have been previously described [1].

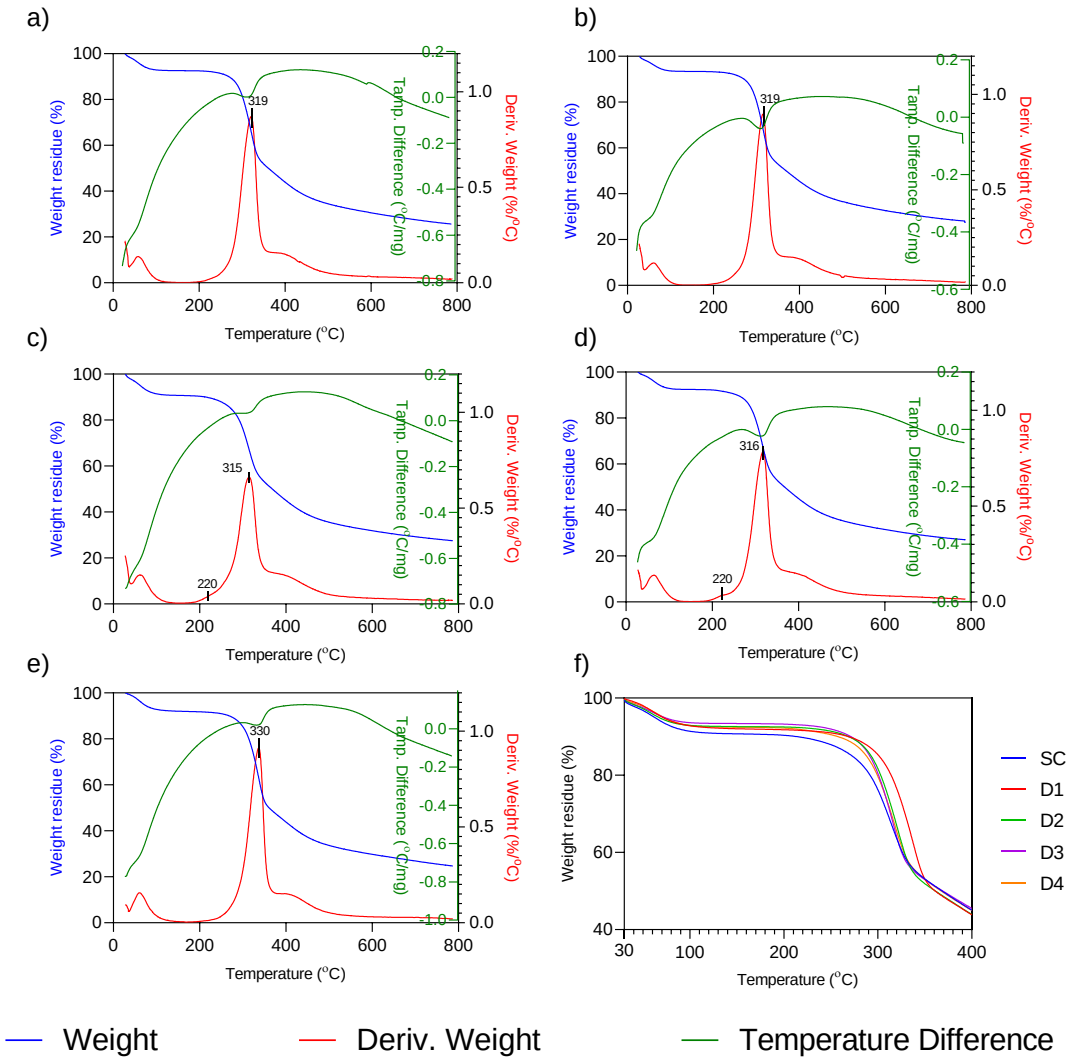

Figure 4. TGA and DSC analysis of the SC and SF after the different degumming process: a) SC; b) D1, Autoclave; c) D2, Na2CO3 30´; d) D3, Na2CO3 120´; e) D4, Ultrasounds and f) comparison of TGA curves of all samples. *(Please refer to the online version for the color representation of the figure.)*

3.6. Size and morphology of the SFNs

The four degummed SFs were processed to produce SFNs as stated in the experimental section, and their hydrodynamic features were determined by DLS to assess how the degumming process affects the final size distribution, polydispersity index (PdI), Z-potential and surface charge density of nanoparticles. The size distribution and FESEM images of the SFNs are shown in Figure 5 and the values of Z-average (d.nm) and PdI, calculated with the cumulant approach, are presented in Table 3. All SFNs presented a monomodal size distribution with low values of PdI (<0.2). FESEM images of the SFN are also shown in Figure 5. In the dried state, the SFNs appeared as nanoparticle clusters. However, FESEM images revealed the almost spherical morphology of the nanoparticles.

Preprints (www.preprints.org) | NOT PEER-REVIEWED | Posted: 6 November 2019 doi:10.20944/preprints201911.0049.v1

Peer-reviewed version available at Polymers 2019, 11, 2045; doi:10.3390/polym11122045

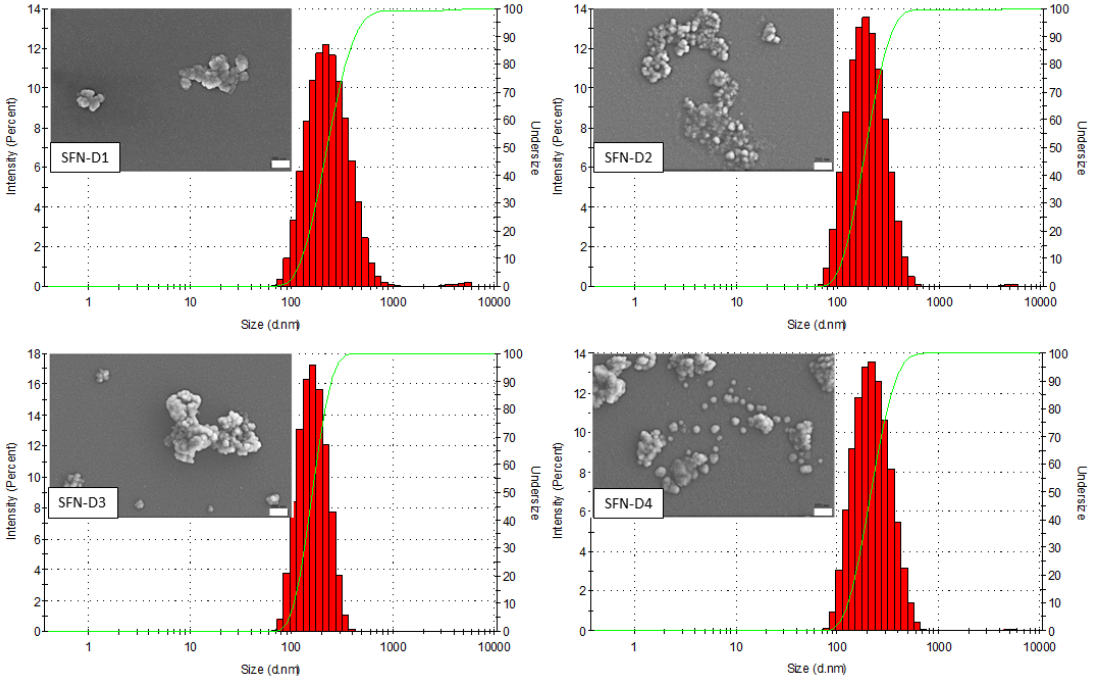

Figure 5. Size distributions by intensity measured in DLS with the corresponding FESEM images of SFN prepared from SF degummed by: D1) Autoclave, D2) Na2CO3 30′, D3) Na2CO3 120′ and D4) Ultrasounds. Scale bar=200 nm. *(Please refer to the online version for the color representation of the figure.)*

Nonetheless, there were significant differences in both Z-Average and size distributions among the SFN samples ($p < 0.05$). As depicted in Table 3, both the Z-average and PdI of the nanoparticles varied in the order: D1>D4>D2>D3. D3-SFN presented the narrowest size distribution and the smallest Z-average of all samples, and this correlates with the highest degradation of SF peptides observed in the gel analysis. Thus, the length of the peptide chains would affect the final size of the nanoparticles. The smaller the size of the peptide chains, the smaller the resultant nanoparticles.

Table 3. Hydrodynamic size, Polydispersity Index and Z-potential of SFN obtained by using SF from the following degumming process: D1) Autoclave, D2) Na2CO3 30′, D3) Na2CO3 120′ and D4) Ultrasound.

Sample	Z-Average (nm)[a]	PdI	Z-potential (mV)[a]	Surface charge density (C/m^2)	Negative charges (mM/g)
SFN-D1	214 ± 4	0.185 ± 0.003	-26.4 ± 0.5	$-2.16 \pm 0.04 \cdot 10^{-3}$	$4{,}48\ 10^{-1}$
SFN-D2	179 ± 1	0.146 ± 0.008	-30.2 ± 1.6	$-2.53 \pm 0.12 \cdot 10^{-3}$	$6{,}29\ 10^{-1}$
SFN-D3	156 ± 3	0.087 ± 0.002	-30.2 ± 1.8	$-2.57 \pm 0.06 \cdot 10^{-3}$	$7{,}31\ 10^{-1}$
SFN-D4	207 ± 4	0.152 ± 0.004	-24.7 ± 1.6	$-2.01 \pm 0.06 \cdot 10^{-3}$	$4.32\ 10^{-1}$

[a]Results are shown as mean ± standard deviation, $n = 3$.

All samples showed a negative Z-potential ranging from -24.7 to -30.2 mV (Table 3) that support the stability of the aqueous suspensions of nanoparticles due the electrostatic repulsion forces among particles negatively charged. The nanoparticles obtained from the both alkaline degummed SF showed similar Z-potentials, but higher in absolute value than the "water only" treatments. This fact

can be explained by the higher pH value of the solvent in the treatment, which could produce a highest number of deprotonated carboxyl groups, conferring a more negative net charge to the SFNs.

The surface charge density can be more descriptive of the effect of the degumming treatment on the characteristics of the nanoparticles because not only the Z-potential but also the size of the nanoparticles are variables in the calculation of the surface charge density. As can be seen on table 3, the surface charge density reaches values of about $2.5 \cdot 10^{-3}$ C/m^2. The nanoparticles obtained from degummed fibroins in water-only treatments presented a lower density around $2.0 \cdot 10^{-3}$ C/m^2. Considering the nanoparticles as spheres with a diameter equivalent to the Z-average, the concentration of negative charges per unit of mass can be calculated which ranged from $7{,}31 \cdot 10^{-1}$ μmol/g for SFN-D3 to $4{,}32 \cdot 10^{-1}$ for SFN-D4. Differences in the number of solvent accessible carboxylate groups have remarkable effect on the functionalization of the surface by using carbodiimide coupling chemistry.

4. Conclusions

The main aim of this work was to study the effects of four degumming methods, namely autoclaving, short and intensive alkaline boiling (30 and 120 min, respectively) and high-power ultrasounds on SF integrity and consequently on the formed SFN. It was hypothesized that with a higher degradation, smaller nanoparticles could be achieved, due to the smaller polymer chains used as building blocks.

The integrity of SF was analyzed by gel electrophoresis, whereby smaller molecular weight distributions were interpreted as reflecting a higher degree of degradation. The autoclave method was the least aggressive as regards SF integrity, while yielding good SS removal. Alkaline methods were seen to be more aggressive with the SF compared to the rest of the treatments. An increase in alkali processing time, increased SF degradation, further reducing the molecular weight distribution, as expected. While small quantities of SS were detected when SF fibers were treated with the mild process, no remaining SS was observed after the long process. The ultrasound method underperformed in terms of SS removal in the experimental conditions of this work but produced comparatively lower damage to the SF fibers. An overall increase in β-sheet structure was observed during SFN preparation, with the consequent reduction of less ordered structures (◎-helix or random coil).

There was a positive correlation between SF degradation and a reduction in the mean size and size distribution of SFN. However, the significant changes in Z-potential and surface charges density between SFNs coming from different treatments can be attributed to the nature of the degumming solvents (i. e. alkaline solution or ultrapure water). It was also observed that the remaining SS could interfere in SFN formation, leading to a lower ◎-sheet content but with no effect on size was observed.

For the design and synthesis of efficient drug delivery systems, alkaline treatment D3 is the most effective degumming process, not only because of the size and Z-potential, but also because the increase of carboxyl groups in SFN-D3 improves the capability of the functionalization of the particle surface by carbodiimide coupling, providing a more favorable surface as nanocarrier-based drug delivery system.

As a final remark, the degumming method implemented for SF purification must be taken into account as a key step in the protocol used for SFN preparation, as the integrity of the protein and the presence of SS affect to the mean size, the size distribution and the surface charge density of the particles.

Supplementary Materials: The following are available online at www.mdpi.com/xxx/s1, Figure S1: Example of base line traced in Amide III absorption band for the crystallinity index calculation, Table S1: Assignment of the vibration bands in Amide I, Figure S2: FSD of Amide I absorption band and example of band fitting, Table S2: List of parameters used to calculate the surface charge density, Table S3: Degumming efficiency expressed in terms of mass loss and Crystallinity index (CI) of SF samples: D1) Autoclave, D2) Na2CO3 30′, D3) Na2CO3 120′ and D4) Ultrasounds, Table S4: Relative contribution of secondary structure features of the Amide I in the different stages of the process. SC) Silk Cocoons, internal or external faces, SF) Degummed silk fibroin and SFN)

Silk fibroin nanoparticles prepared from SF degummed by: D1) Autoclave, D2) Na2CO3 30′, D3) Na2CO3 120′ and D4) Ultrasound obtained by FSD analysis of the Amide I infrared absorption band. n = 3, average ± standard deviation, Table S5: Analysis of variance (ANOVA) of the relative contribution of secondary structure (n = 3).

Author Contributions: G.C. and A.A.L.P. designed the experiment, collaborated in silk degumming, silk processing, nanoparticle preparation and characterization and drafting the manuscript, M.G.M. contributed to the characterization of the nanoparticles and contributed to the writing and correction of the draft, S.D.A.C. was in charge of raising silkworms, cocoon stifling and contributed to the writing and correction of the draft, J.L.C., head of the research team at IMIDA and G.V, head of the research team at University of Murcia, supervised all the work during its development and contributed to the writing and correction of the draft. All authors contributed with text and/or comments to the manuscript and approved the final version.

Funding: This work has been partially supported (80%) from the European Commission ERDF/FEDER Operational Programme 'Murcia' CCI Nº 2007ES161PO001 (Project No. 14-20/20), and the Spanish MINECO (Ref. CTQ2017-87708-R) and the programme of support to the research of the Seneca Foundation of Science and Technology of Murcia, Spain (Ref. 20977/PI/18). Dr. Lozano-Pérez's research contract was partially supported (80%) by the ERDF/FEDER Operational Programme 'Murcia' CCI Nº 2007ES161PO001 (Project No. 14-20/20),. M. G. Montalbán's research contract is founded by the Spanish MINECO (Juan de la Cierva-Formación contract, Ref. FJCI-2016-28081). Dr. Salvador D. Aznar-Cervantes's research contract is founded by the program INIA-CCAA (DOC INIA 2015), announced by the National Institute for Agricultural and Food Research and Technology (INIA) and supported by The Spanish State Research Agency (AEI) under the Spanish Ministry of Economy, Industry and Competitiveness.

Acknowledgments: AALP, MGM and SDAC acknowledges the financial support for their research contracts.

Conflicts of Interest: The authors declare no conflict of interest.

References

[1] S. Mazzi, E. Zulker, J. Buchicchio, B. Anderson, X. Hu, Comparative thermal analysis of Eri, Mori, Muga, and Tussar silk cocoons and fibroin fibers, J. Therm. Anal. Calorim. 116 (2014) 1337–1343. doi:10.1007/s10973-013-3631-0.

[2] D.N. Rockwood, R.C. Preda, T. Yücel, X. Wang, M.L. Lovett, D.L. Kaplan, Materials fabrication from *Bombyx mori* silk fibroin, Nat. Protoc. 6 (2011) 1612–31. doi:10.1038/nprot.2011.379.

[3] A. Ajisawa, Dissolution of silk fibroin with calciumchloride/ethanol aqueous solution, J. Seric. Sci. Jpn. 67 (1998) 91–94.

[4] D.M. Phillips, L.F. Drummy, D.G. Conrady, D.M. Fox, R.R. Naik, M.O. Stone, P.C. Trulove, H.C. De Long, R.A. Mantz, Dissolution and Regeneration of *Bombyx mori* Silk Fibroin Using Ionic Liquids, J. Am. Chem. Soc. 126 (2004) 14350–14351. doi:10.1021/ja046079f.

[5] M. Montalbán, J. Coburn, A. Lozano-Pérez, J. Cenis, G. Víllora, D. Kaplan, Production of Curcumin-Loaded Silk Fibroin Nanoparticles for Cancer Therapy, Nanomaterials. 8 (2018) 126. doi:10.3390/nano8020126.

[6] F.J. Hernández-Fernández, A.P. de los Ríos, F. Tomás-Alonso, D. Gómez, M. Rubio, G. Víllora, Integrated reaction/separation processes for the kinetic resolution of rac-1-phenylethanol using supported liquid membranes based on ionic liquids, Chem. Eng. Process. Process Intensif. 46 (2007) 818–824. doi:10.1016/j.cep.2007.05.014.

[7] F.J. Hernández-Fernández, A.P. de los Ríos, F. Tomás-Alonso, D. Gómez, G. Víllora, On the development of an integrated membrane process with ionic liquids for the kinetic resolution of rac-2-pentanol, J.

Memb. Sci. 314 (2008) 238–246. doi:10.1016/j.memsci.2008.01.043.

[8] R.D. Rogers, K.R. Seddon, Ionic Liquids - Solvents of the Future?, Science (80-.). 302 (2003) 792–793. doi:10.1126/science.1090313.

[9] D.M. Phillips, L.F. Drummy, D.G. Conrady, D.M. Fox, R.R. Naik, M.O. Stone, P.C. Trulove, H.C. De Long, R.A. Mantz, Dissolution and Regeneration of Bombyx mori Silk Fibroin Using Ionic Liquids, (2004) 14350–14351.

[10] D.N. Rockwood, R.C. Preda, T. Yücel, X. Wang, M.L. Lovett, D.L. Kaplan, Materials fabrication from Bombyx mori silk fibroin, Nat. Protoc. 6 (2011) 1612–1631. doi:10.1038/nprot.2011.379.

[11] H. Wang, Y. Zhang, H. Shao, X. Hu, A study on the flow stability of regenerated silk fibroin aqueous solution, Int. J. Biol. Macromol. 36 (2005) 66–70. doi:10.1016/j.ijbiomac.2005.03.011.

[12] S.D. Aznar-Cervantes, A.A. Lozano-Pérez, M. García Montalbán, G. Víllora, D. Vicente-Cervantes, J.L. Cenis, Importance of refrigeration time in the electrospinning of silk fibroin aqueous solutions, J. Mater. Sci. 50 (2015) 4879–4887. doi:10.1007/s10853-015-9032-y.

[13] A.A. Lozano-Pérez, M.G. Montalbán, S.D. Aznar-Cervantes, F. Cragnolini, J.L. Cenis, G. Víllora, Production of silk fibroin nanoparticles using ionic liquids and high-power ultrasounds, J. Appl. Polym. Sci. 132 (2014) n/a-n/a. doi:10.1002/app.41702.

[14] Y.-J. Wang, Y.-Q. Zhang, Three-layered sericins around the silk fibroin fiber from *Bombyx mori* cocoon and their amino acid composition, Adv. Mater. Res. 175–176 (2011) 158–163. doi:10.4028/www.scientific.net/AMR.175-176.158.

[15] H.J. Kim, M.K. Kim, K.H. Lee, S.K. Nho, M.S. Han, I.C. Um, Effect of degumming methods on structural characteristics and properties of regenerated silk, Int. J. Biol. Macromol. 104 (2017) 294–302. doi:10.1016/j.ijbiomac.2017.06.019.

[16] Y. Wang, J. Guo, L. Zhou, C. Ye, F.G. Omenetto, D.L. Kaplan, S. Ling, Design, Fabrication, and Function of Silk-Based Nanomaterials, Adv. Funct. Mater. 28 (2018) 1–24. doi:10.1002/adfm.201805305.

[17] R. Wang, Y. Zhu, Z. Shi, W. Jiang, X. Liu, Q.Q. Ni, Degumming of raw silk via steam treatment, J. Clean. Prod. 203 (2018) 492–497. doi:10.1016/j.jclepro.2018.08.286.

[18] F. Wang, Y.Q. Zhang, Effects of alkyl polyglycoside (APG) on Bombyx mori silk degumming and the mechanical properties of silk fibroin fibre, Mater. Sci. Eng. C. 74 (2017) 152–158. doi:10.1016/j.msec.2017.02.015.

[19] T.T. Cao, Y.Q. Zhang, Processing and characterization of silk sericin from Bombyx mori and its application in biomaterials and biomedicines, Mater. Sci. Eng. C. 61 (2016) 940–952. doi:10.1016/j.msec.2015.12.082.

[20] L. Wang, Z. Luo, Q. Zhang, Y. Guan, J. Cai, R. You, X. Li, Effect of Degumming Methods on the Degradation Behavior of Silk Fibroin Biomaterials, Fibers Polym. 20 (2019) 45–50. doi:10.1007/s12221-

019-8658-9.

[21] G. Freddi, R. Mossotti, R. Innocenti, Degumming of silk fabric with several proteases, J. Biotechnol. 106 (2003) 101–112. doi:10.1016/j.jbiotec.2003.09.006.

[22] J. Pérez-Rigueiro, M. Elices, J. Llorca, C. Viney, Effect of degumming on the tensile properties of silkworm (*bombyx mori*) silk fiber, J. Appl. Polym. Sci. 84 (2002) 1431–1437. doi:10.1002/app.10366.

[23] M. Yuksek, D. Kocak, A. Beyit, N. Merdan, Effect of Degumming Performed with Different Type Natural Soaps and Through, 6 (2012) 801–808. doi:10.1006/mthe.2002.0675.

[24] N.M. Mahmoodi, F. Moghimi, M. Arami, F. Mazaheri, Silk degumming using microwave irradiation as an environmentally friendly surface modification method, Fibers Polym. 11 (2010) 234–240. doi:10.1007/s12221-010-0234-2.

[25] G. Genç, G. Narin, O. Bayraktar, Spray drying as a method of producing silk sericin powders, J. Achiev. Mater. Manuf. Eng. 37 (2009) 78–86.

[26] A.R. Lalit Jajpura, The Biopolymer Sericin: Extraction and Applications, J. Text. Sci. Eng. 05 (2015) 1–5. doi:10.4172/2165-8064.1000188.

[27] S.D. Aznar-Cervantes, D. Vicente-Cervantes, L. Meseguer-Olmo, J.L. Cenis, A.A. Lozano-Pérez, Influence of the protocol used for fibroin extraction on the mechanical properties and fiber sizes of electrospun silk mats, Mater. Sci. Eng. C. 33 (2013) 1945–1950. doi:10.1016/j.msec.2013.01.001.

[28] K. Nultsch, O. Germershaus, Silk fibroin degumming affects scaffold structure and release of macromolecular drugs, Eur. J. Pharm. Sci. 106 (2017) 254–261. doi:10.1016/j.ejps.2017.06.012.

[29] M.L. Gulrajani, S.V. Gupta, A. Gupta, M. Suri, Degumming of silk with different protease enzymes, Indian J. Fibre Text. Res. 21 (1996) 270–275.

[30] G. Freddi, G. Allera, G. Candiani, Degumming of silk fabrics with tartaric acid, J. Soc. Dye. Colour. 112 (2008) 191–195. doi:10.1111/j.1478-4408.1996.tb01817.x.

[31] M.M.R. Khan, M. Tsukada, Y. Gotoh, H. Morikawa, G. Freddi, H. Shiozaki, Physical properties and dyeability of silk fibers degummed with citric acid, Bioresour. Technol. 101 (2010) 8439–8445. doi:10.1016/j.biortech.2010.05.100.

[32] H.Y. Wang, Y.Q. Zhang, Effect of regeneration of liquid silk fibroin on its structure and characterization, Soft Matter. 9 (2013) 138–145. doi:10.1039/c2sm26945g.

[33] F. Wang, T.T. Cao, Y.Q. Zhang, Effect of silk protein surfactant on silk degumming and its properties, Mater. Sci. Eng. C. 55 (2015) 131–136. doi:10.1016/j.msec.2015.05.041.

[34] Z. Wang, H. Yang, W. Li, C. Li, Effect of silk degumming on the structure and properties of silk fibroin, J. Text. Inst. 5000 (2018) 1–7. doi:10.1080/00405000.2018.1473074.

[35] B.J. Allardyce, R. Rajkhowa, R.J. Dilley, M. Atlas, J. Kaur, X. Wang, The impact of degumming conditions

on the properties of silk films for biomedical applications, Text. Res. J. 0 (2015) 1–13. doi:10.1177/0040517515586166.

[36] J.H. Lee, D.W. Song, Y.H. Park, I.C. Um, Effect of residual sericin on the structural characteristics and properties of regenerated silk films, Int. J. Biol. Macromol. 89 (2016) 273–278. doi:10.1016/j.ijbiomac.2016.04.073.

[37] B.K. Park, I.C. Um, Effect of molecular weight on electro-spinning performance of regenerated silk, Int. J. Biol. Macromol. 106 (2018) 1166–1172. doi:10.1016/j.ijbiomac.2017.08.115.

[38] Z. Zhao, Y. Li, M.-B. Xie, Silk Fibroin-Based Nanoparticles for Drug Delivery, Int. J. Mol. Sci. 16 (2015) 4880–4903. doi:10.3390/ijms16034880.

[39] Q. Liu, H. Liu, Y. Fan, Preparation of silk fibroin carriers for controlled release, Microsc. Res. Tech. 80 (2017) 312–320. doi:10.1002/jemt.22606.

[40] F. Mottaghitalab, M. Farokhi, M.A. Shokrgozar, F. Atyabi, H. Hosseinkhani, Silk fibroin nanoparticle as a novel drug delivery system, J. Control. Release. 206 (2015) 161–176. doi:10.1016/j.jconrel.2015.03.020.

[41] M.G. Montalbán, G. Carissimi, A.A. Lozano-Pérez, J.L. Cenis, J.M. Coburn, D.L. Kaplan, G. Víllora, Biopolymeric Nanoparticle Synthesis in Ionic Liquids, in: Recent Adv. Ion. Liq., InTech, 2018: pp. 3–26. doi:10.5772/intechopen.78766.

[42] S.D. Aznar-cervantes, A. Abel, M. García, G. Víllora, Importance of refrigeration time in the electrospinning of silk fibroin aqueous solutions, 50 (2015) 4879–4887. doi:10.1007/s10853-015-9032-y.

[43] S.D. Aznar-cervantes, D. Vicente-cervantes, A.A. Lozano-pérez, L. Meseguer-olmo, J.L. Cenis, Influence of the Protocol Used for Fibroin Extraction on the Mechanical Properties and Fiber Sizes of Electrospun Silk Mats, (n.d.).

[44] S.D. Aznar-Cervantes, A. Pagan, B. Monteagudo Santesteban, J.L. Cenis, Effect of different cocoon stifling methods on the properties of silk fibroin biomaterials, Sci. Rep. 9 (2019) 1–11. doi:10.1038/s41598-019-43134-5.

[45] S.D. Aznar-Cervantes, A. Pagan, B. Monteagudo Santesteban, J.L. Cenis, Effect of different cocoon stifling methods on the properties of silk fibroin biomaterials, Sci. Rep. 9 (2019) 6703. doi:10.1038/s41598-019-43134-5.

[46] U.K. Lammli, Cleavage of Structural Proteins during the Assembly of the Head of Bacteriophage T4, Nature. 227 (1970) 680–685.

[47] N. V. Bhat, G.S. Nadiger, Crystallinity in silk fibers: Partial acid hydrolysis and related studies, J. Appl. Polym. Sci. 25 (1980) 921–932. doi:10.1002/app.1980.070250518.

[48] G.S. Nadiger, N. V. Bhat, Effect of plasma treatment on the structure and allied textile properties of mulberry silk, J. Appl. Polym. Sci. 30 (1985) 4127–4135. doi:10.1002/app.1985.070301014.

[49] X. Hu, D. Kaplan, P. Cebe, Determining beta-sheet crystallinity in fibrous proteins by thermal analysis and infrared spectroscopy, Macromolecules. 39 (2006) 6161–6170. doi:10.1021/ma0610109.

[50] A. Barth, C. Zscherp, What vibrations tell us about proteins, Q. Rev. Biophys. 35 (2002) 369–430. doi:10.1017/S0033583502003815.

[51] K. Makino, H. Ohshima, Electrophoretic mobility of a colloidal particle with constant surface charge density, Langmuir. 26 (2010) 18016–18019. doi:10.1021/la1035745.

[52] Y.Q. Zhang, Applications of natural silk protein sericin in biomaterials, Biotechnol. Adv. 20 (2002) 91–100. doi:10.1016/S0734-9750(02)00003-4.

[53] M. Mondal, K. Trivedy, S.N. Kumar, The silk protein,sericin and fibroin in silkworm,Bombyx mori Linn,-a review, Casp. J Env Sci. 5 (2007) 63–76. doi:http://dx.doi.org/10.1016/S0141-8130(99)00005-7.

[54] B. Lotz, F. Colonna Cesari, The chemical structure and the crystalline structures of *bombyx mori* silk fibroin, Biochimie. 61 (1979) 205–214. doi:10.1016/S0300-9084(79)80067-X.

[55] S. Ling, Z. Qi, D.P. Knight, Z. Shao, X. Chen, Synchrotron FTIR microspectroscopy of single natural silk fibers, Biomacromolecules. 12 (2011) 3344–3349. doi:10.1021/bm2006032.

[56] M.A. Koperska, D. Pawcenis, J. Bagniuk, M.M. Zaitz, M. Missori, T. Łojewski, J. Łojewska, Degradation markers of fibroin in silk through infrared spectroscopy, Polym. Degrad. Stab. 105 (2014) 185–196. doi:10.1016/j.polymdegradstab.2014.04.008.

[57] R.E. Marsh, R.B. Corey, L. Pauling, An Investigation of the structure of solk fibroin*, 16 (1955). doi:10.1016/0006-3002(55)90178-5.

[58] G.H. Altman, F. Diaz, C. Jakuba, T. Calabro, R.L. Horan, J. Chen, H. Lu, J. Richmond, D.L. Kaplan, Silk-based biomaterials, Biomaterials. 24 (2003) 401–416. doi:10.1016/S0142-9612(02)00353-8.

[59] J. Shao, J. Zheng, J. Liu, C.M. Carr, Fourier transform Raman and Fourier transform infrared spectroscopy studies of silk fibroin, J. Appl. Polym. Sci. 96 (2005) 1999–2004. doi:10.1002/app.21346.

[60] P. Garside, P. Wyeth, Crystallinity and degradation of silk: correlations between analytical signatures and physical condition on ageing, Appl. Phys. A. 89 (2007) 871–876. doi:10.1007/s00339-007-4218-z.

[61] X. Hu, D. Kaplan, P. Cebe, Dynamic Protein-Water Relationships during Beta Sheet Formation Dynamic Protein - Water Relationships during -Sheet Formation, (2016) 3939–3948. doi:10.1021/ma071551d.

[62] Y. Yang, J. Chen, W. Bonani, B. Chen, S. Eccheli, D. Maniglio, C. Migliaresi, A. Motta, Sodium oleate induced rapid gelation of silk fibroin, J. Biomater. Sci. Polym. Ed. 29 (2018) 1219–1231. doi:10.1080/09205063.2018.1452417.

[63] T. Wongpinyochit, B.F. Johnston, F.P. Seib, Degradation Behavior of Silk Nanoparticles - Enzyme Responsiveness, ACS Biomater. Sci. Eng. 4 (2018) 942–951. doi:10.1021/acsbiomaterials.7b01021.

[64] M. Nakpathom, B. Somboon, N. Narumol, Z. Wang, Y. Zhang, J. Zhang, L. Huang, J. Liu, Y. Li, G. Zhang,

S.C. Kundu, L. Wang, Exploring natural silk protein sericin for regenerative medicine: An injectable, photoluminescent, cell-adhesive 3D hydrogel, Sci. Rep. 4 (2014) 1–11. doi:10.1038/srep07064.

[65] M. Nakpathom, B. Somboon, N. Narumol, Exploring natural silk protein sericin for regenerative medicine: An injectable, photoluminescent, cell-adhesive 3D hydrogel, J. Microsc. Soc. Thail. 23 (2009) 142–146.

[66] T.M. Bawazeer, M.S. Alsoufi, Surface Characterization and Properties of Raw and Degummed (*Bombyx mori*) Silk Fibroin Fiber toward High Performance Applications of *"Kisswa Al- Kabba,"* Int. J. Curr. Res. 9 (2017) 48335–48343.

[67] C.Z. Zhou, F. Confalonieri, M. Jacquet, R. Perasso, Z.G. Li, J. Janin, Silk fibroin: Structural implications of a remarkable amino acid sequence, Proteins Struct. Funct. Genet. 44 (2001) 119–122. doi:10.1002/prot.1078.

[68] S. Inoue, K. Tanaka, F. Arisaka, S. Kimura, K. Ohtomo, S. Mizuno, Silk fibroin of Bombyx mori is secreted, assembling a high molecular mass elementary unit consisting of H-chain, L-chain, and P25, with a 6:6:1 molar ratio, J. Biol. Chem. 275 (2000) 40517–40528. doi:10.1074/jbc.M006897200.

[69] Y. Takasu, H. Yamada, K. Tsubouchi, Isolation of three main sericin components from the cocoon of the silkworm, Bombyx mori., Biosci. Biotechnol. Biochem. 66 (2002) 2715–2718. doi:10.1271/bbb.66.2715.

[70] Y.-Q. Zhang, W.-D. Shen, R.-L. Xiang, L.-J. Zhuge, W.-J. Gao, W.-B. Wang, Formation of silk fibroin nanoparticles in water-miscible organic solvent and their characterization, J. Nanoparticle Res. 9 (2007) 885–900. doi:10.1007/s11051-006-9162-x.